



HAL
open science

Experimental study and numerical simulation of preform or sheet infra-red radiative heating

Serge Monteix, Fabrice Schmidt, Yannick Le Maout

► To cite this version:

Serge Monteix, Fabrice Schmidt, Yannick Le Maout. Experimental study and numerical simulation of preform or sheet infra-red radiative heating. AMPT'99 -Advances in Materials and Processing Technologies, Aug 1999, Dublin, Iran. 10 p. hal-01799141

HAL Id: hal-01799141

<https://hal.science/hal-01799141>

Submitted on 15 Mar 2019

HAL is a multi-disciplinary open access archive for the deposit and dissemination of scientific research documents, whether they are published or not. The documents may come from teaching and research institutions in France or abroad, or from public or private research centers.

L'archive ouverte pluridisciplinaire **HAL**, est destinée au dépôt et à la diffusion de documents scientifiques de niveau recherche, publiés ou non, émanant des établissements d'enseignement et de recherche français ou étrangers, des laboratoires publics ou privés.

EXPERIMENTAL STUDY AND NUMERICAL SIMULATION OF PREFORM OR SHEET INFRA-RED RADIATIVE HEATING

S. Monteix¹, F. Schmidt¹, Y. Le Maoult¹

1. Ecole des Mines d'Albi Carmaux, France

ABSTRACT

A critical stage of both the injection-stretch blow moulding and thermoforming processes is the heating stage, as the final part thickness distribution is strongly dependent on the preform or sheet temperature distribution prior to forming.

Optimisation of the infrared oven is therefore necessary. Experiments have been conducted in order to characterise the heat source of the infrared emitter and the interaction between the heaters and a semi-transparent PET sheet. An 880 LW AGEMA infrared camera has been used to evaluate the surface distribution of the transmitted heat flux by measuring the temperature distribution on the surface of the thermoplastic sheet. In addition, numerical simulations using control-volume method have been carried out and compared with experimental data.

KEYWORDS:

Contour integration method, control-volume method, heating stage, infrared camera, stretch-blow moulding, thermoforming, view factor computation.

1. INTRODUCTION

In both the injection stretch-blow moulding and thermoforming processes, a tube-shaped or sheet-shaped thermoplastic preform (PET, PVC, PP,...) must be heated before forming. In order to increase the temperature of the preform above the glass transition, infrared ovens are used [1]. Infrared heating permits a rapid heating with an important heat flux (proportional at the fourth power of the source temperature), even on the inner surface far from the incident radiative source.

As the final thickness distribution of the part is dependent on the initial temperature distribution inside the preform, it is very important to investigate influent parameters describing the heating stage. They depend both on the geometrical and spectral interactions between lamps and irradiated plastic materials.

Consequently of the specific interaction, the ratio between electric power and absorbed energy in the PET tubular preform is approximately 20%. Optimisation of the infrared oven is then necessary to allow for a control of the temperature distribution and also for a minimisation of the energy costs. In this way, the following methodology has been applied on the heating of P.E.T sheets :

- Characterisation of infrared heaters ;
- Measurement of the surface temperature distribution ;
- Development of a 3D control-volume model of the heating stage.

2. CHARACTERIZATION OF THE HEAT SOURCE

The spectral properties of the infrared heaters have already been determined in previous papers [2,3]. The infrared lamps used are sketched in Figure 1.

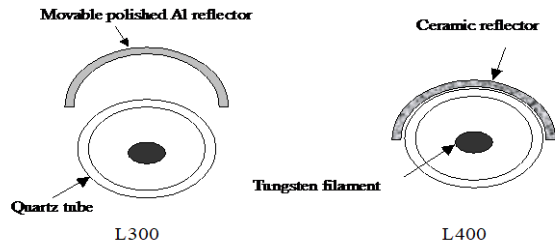


Fig. 1-Infrared heaters

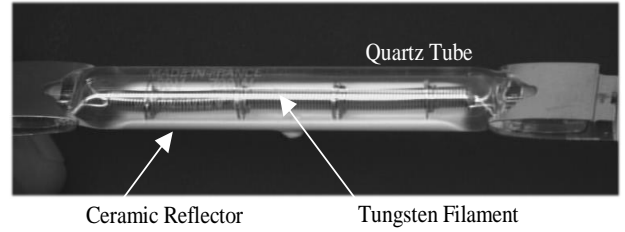


Fig. 2-Industrial heater (L400)

They are composed of a coiled tungsten filament, contained in a quartz tubular enclosure and a reflector in order to increase the heat flux efficiency to the product.

The lamp called respectively, L300 and L400 present a nominal electric power of 300W and 700W. The L300 is used with a cylindrical reflector made in polished aluminium. The second one L400 commonly plugged in industrial oven, is fitted with a reflector made of a ceramic coating on the back side of the quartz tube in Figure2.

With a characteristic electrical power in range, and a characteristic resistivity the tungsten filament reaches in steady state, for the L300 at 300W, a temperature about 2300K, and for the L400 used at 400W a temperature about 1700K.

An experimental set-up (see Figure 3), using a thermopile detector (remote sensing heat flux), was developed in order to measure the spatial directivity of the lamp.

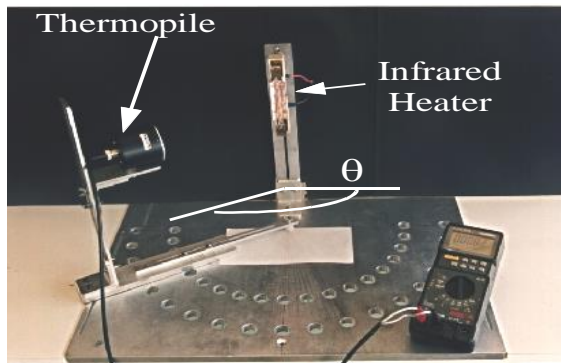


Fig. 3-Experimental set-up for infrared heaters characterisation.

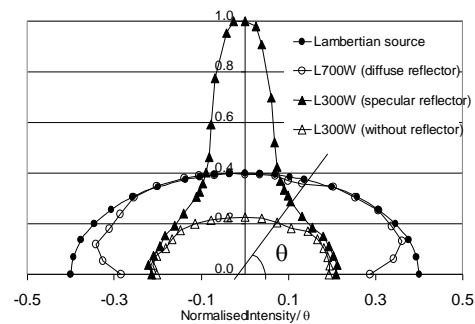


Fig.4-Infrared heater's directivity

The flux sensor moves on a half circle around the filament, in order to measure the spatial directivity of each heater. Then it intercepts the radiation, in each direction described by the angle θ . The thermopile presents a bandwidth defined between 8-14 μm . In this spectral range, the quartz tube presents a full absorption of the filament radiation [2]. We assume that the heaters directivity is the same as the quartz tube because of their concentric geometry (the cylindrical filament in the quartz tube).

In Figure 4, the normalised intensity is plotted versus the angle θ . For all the measurement, the solid angle of the thermopile is centred on the middle of the lamp filament. In comparison with a Lambertian source (diffuse radiation), the Lamp L400 and the L300 used without reflector

is similar to an isotropic source (except some border's effects). As expected, we observe that the lamp L300 fitted with a specular reflector exhibits a strong directionality in front of the reflector.

3. TEMPERATURE DISTRIBUTION MEASUREMENT

3.1 Experimental Procedure

Figure 5 shows the experimental set-up, which has been developed in order to measure the surface temperature evolution, when a PET sheet is heating using previous infrared lamp.

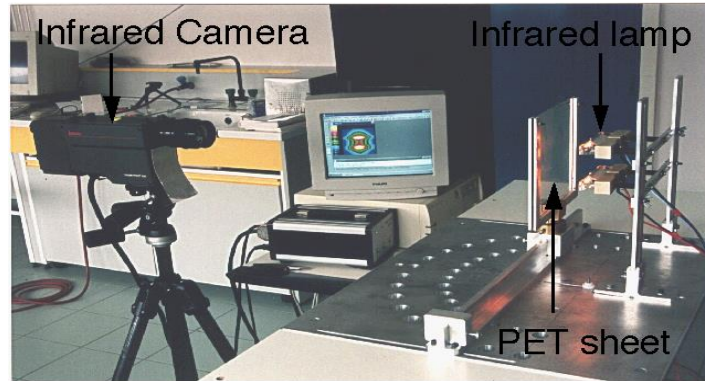


Fig. 5-Experimental heating set-up

An 880 LW AGEMA infrared camera (8-12 μm bandwidth) is used to evaluate in a remote sensing, the spatial and transient temperature distribution. The surface dimension of the sheet is 20cm x 20cm and the thickness is 1.5 mm. The distance between heaters and sheets is 5 cm. The frequency of analysis is 25 frames per second and the device is connected to a 12 bit data acquisition board drive with a real time software.

The camera's objective is oriented normally to the sheet's surface. However, due to the spectral absorbance of the PET [4], we have to take care of this participating media, in order to secure the surface temperature measurement [5]. To do this, the spectral absorbance of the PET must be characterised previously to determine the bandwidth where the material is assumed to be opaque (see Figure 6). For which, only the radiation emitted from the material surface is intercepted by the camera's sensor, although all the other radiation from the bulk or the sheet environment are absorbed, before reaching the viewed surface [6].

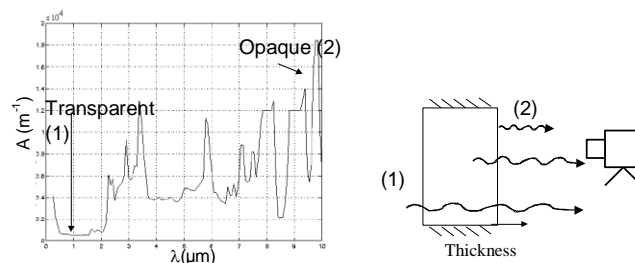


Fig. 6-The PET spectral absorbance

Previous work deals with PET transmittivity [7], in the spectral range of the heaters intensity, defined by the Wien's law for a used temperature about 2300K. In the bandwidth of the camera (8-12 μm) they are no available data. Then in order to observe the PET behaviour, we

have assessed reflectivity and transmittivity coefficients using the infrared camera and a laboratory blackbody.

Tab 1- PET's transmittance [8 ;12] μm
(Black-Body temperature = 150°C)

Thickness (mm)	τ_{sheet}
0,7 mm	$5 \cdot 10^{-3}$
1,5 mm	$2 \cdot 10^{-3}$

Tab 2- Normal PET reflectance [8 ;12] μm .

Black Body Temperature (°C)	ρ_n
70	0,06
110	0,07
150	0,07

Measurements have been processed for 0.7 and 1.5 mm PET sheet thickness. Tab 1 and Tab 2 show a very low average transmittivity on this spectral band. The average emissivity is then calculated from the reflectivity measurement.

Taking into account these characteristics, temperature are measured during heating and cooling stage, from the back and the front surfaces of the sheet. It takes 3 seconds to bring the front face in front of the camera, during wich a cooling stage due to the natural convection occurs.

During this transfer a relative difference less than 0.7 % appears in temperature measurements similar to a cooling with a transfer coefficient h equal to $10 \text{ Wm}^{-1}\text{K}^{-1}$.

In Figure 7, two infrared thermograms are presented for a heating time of 35 seconds.

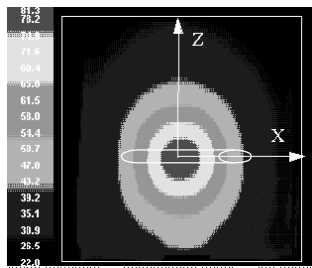


Figure 7-a : Th. with diffuse reflector.

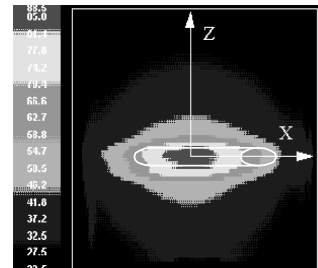


Figure 7-b : Th. with specular reflector

Figure 7.a shows the surface temperature distribution measured on the back face of the sheet for the heat source L400. The surface temperature distribution is relatively isotropic due to the presence of the diffuse reflector. This results confirms that the Lambertian source assumption (diffuse radiation) is valid for the lamp L400. As expected, the surface temperature distribution for the lamp L300 (specular reflector) is strongly anisotropic (see Figure 7.b).

3.2 Results

In this part, thermograms for 1.5 mm PET sheets thickness are examined. Thermograms recorded from the front and the back faces with the same experimental heating conditions provides (Figure 8), the measurement of the temperature gradient, reached across the thickness after an heating time about 35s. This gradient is related to the location of the measured point on the sheet surface in association with the temperature level at this point. The highest gradient (about 8 °C) is reached at the sheet centre (the same as the heater's centre) corresponding to the highest temperature level about 85 °C.

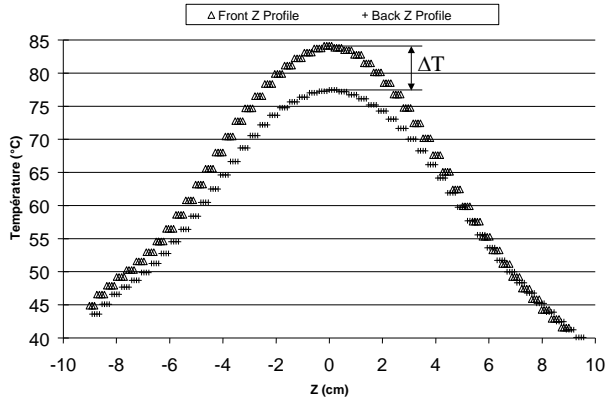


Fig. 8- Measurement of the temperature gradient after heating stop

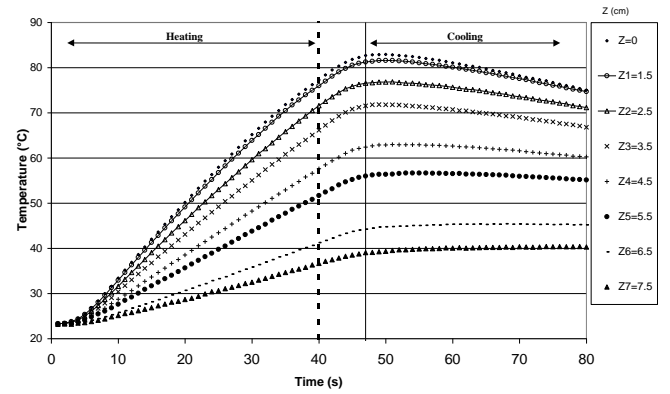


Fig. 9- Transient evolution of the temperature

The temperature versus time is presented in figure 9, from different z- values (see Fig. 7) on the sheet. The dotted line indicates the end of the heating. These measurements during the heating and the cooling stage, reveal a delay between the heater switch-of and the record of the maximum temperature level from the back face. This delay (about 8s) is less important than the time of the diffusion phenomenon in the semi-infinite sheet submitted to a surface temperature T_s . In this case, the time t_{diff} required to reach half the initial temperature difference (between T_s and the temperature at a depth e) is equal to $t_{diff} = \frac{e^2}{0.92\alpha}$, [8].

The PET diffusivity, α is equal to $1.4 \cdot 10^7 \text{ m}^2\text{s}^{-1}$ which corresponds to t_{diff} equal to 17 s. This discrepancy reveals the relative influence of the natural convection, who tends to accelerate the equilibrium of temperature levels across the sheet thickness. In contrary, the spatial temperature distribution after the same equilibrating time presents a larger difference on the z axis. This means the ascendant of the radiative 1D transfer across the thickness on the conduction transfer in 3D.

4. CONTROL -VOLUME FORMULATION

A 3D control-volume model has been developed for computing radiative heat transfer during the infrared heating stage. The sheet-shape domain sketched in Figure 10, is discretised into cubic elements, called control volumes [9].

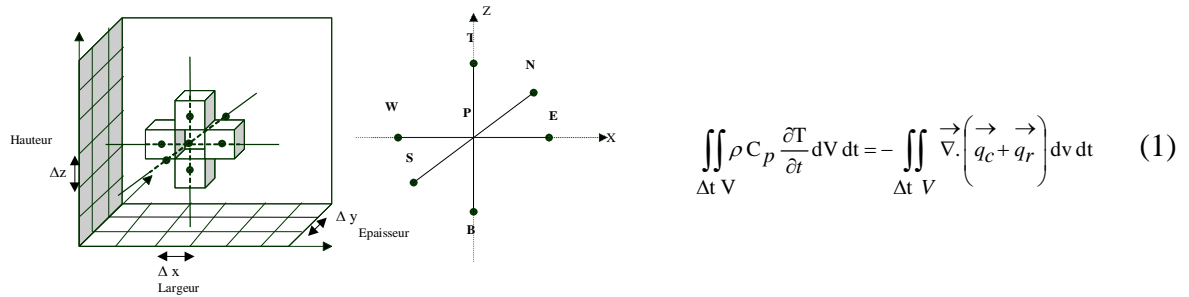


Fig.10-The sheet shape mesh

The temperature balance (Eq.1) including radiative transfer (thermal power absorbed by the polymeric sheet from the infrared heaters) is integrated over each control volume and over the time from t to $t+\Delta t$. $V = \Delta x \Delta y \Delta z$ is the control-volume definition, q_c the Fourier's flux

$$\iint_{\Delta t V} \rho C_p \frac{\partial T}{\partial t} dV dt = - \iint_{\Delta t V} \vec{\nabla} \cdot \left(\vec{q}_c + \vec{q}_r \right) dv dt \quad (1)$$

($\vec{q}_c = -k \nabla T$), q_r the internal radiative heat flux. The unknown temperatures are computed at the cell centres. The heat conductivity k , the specific mass ρ as well as the heat capacity C_p are assumed to be constant, in agreements with previous works [10].

4.1 Internal radiative heat flux

Previous works [11,12] dealt PET sheet's heating with a radiant heat flux, uniform all around the radiated face, or assumed an arbitrary intensity without consideration about heaters dimension. Here, the specific lamp geometry is considered, taking into account from a view factor computation. We assume a constant filament temperature, and then an uniform source temperature. Thus the amount of incident radiation, reaching each front elements of the irradiated sheet, is performed with the contour integration method (Eq.2) using Stoke's theorem [13] :

$$F_{H \rightarrow r_s} = \frac{1}{2\pi S_H} \iint_{\Gamma_H \Gamma_{r_s}} \ln r \, d\vec{r}_H d\vec{r}_{r_s} \quad (2)$$

where the subscripts H refers to the heater and r_s to the sheet front element under consideration ; r is the distance between two elemental linear elements, issued from the discretisation of the entire heater border Γ_H and Γ_{r_s} for each surface of control element's border reaching the irradiated sheet's face. This contour integration method was chosen between different numerical view factor method (Monte-Carlo or geometric method). This method allows a good accuracy at a very low computational time and a simple way of use. An efficient numerical method based on Gaussian quadrature has been applied in order to perform the contour integration.

In order to take into account the participation of the diffuse reflector in the amount of the incident radiation, a coefficient of efficacy k_{rf} is introduced. k_{rf} is calculated, assuming a strip surface for both heater and his reflector, and considering all the flux emitted from this equivalent surface equal to the flux emitted from the entire filament surface [14], i.e. $S_{fil} = \pi d L_{fil}$, where d represents the coiled tungsten diameter equal to 4mm and L_{fil} is the length about 64mm. Using these assumptions k_{rf} is equal to π .

4.2 Amount of incident Radiation

Thus, the amount of incident radiation $\phi(r_s)$ on each surface element is (Eq. 3) :

$$\phi(r_s) = \phi(x, y=0, z) = k_{rf} F_{H \rightarrow r_s} \frac{S_H}{S_{r_s}} \int_{\Delta\lambda} \varepsilon_\lambda(T_{fil}) \pi L_\lambda^0(T_{fil}) d\lambda \quad (3)$$

where $\varepsilon(\lambda)$ is the spectral tungsten emissivity, T_F the filament temperature, L°_λ the black body intensity and λ a given wavelength between [0,2-10] μm .

In a first approximation, internal radiative transfer is assumed to be mono-dimensional across the sheet thickness. The PET bulk temperature ($\approx 400\text{K}$) is very low in comparison to the source temperature ($T_s=1700\text{K}$). So the assumption of "cold material" is convenient. This leads to express the transmitted flux q_r across the thickness (y axis) of the sheet, for an homogenous amorphous PET, using the Beer- Lambert's law in the y direction (Eq.4):

$$q_r = \phi_\lambda(x, y, z) = \phi_\lambda(x, y=0, z) e^{-A_\lambda y} \quad (4)$$

where $A(\lambda)$ is the spectral absorption coefficient of the material (Eq.5) :

$$A(\lambda) = -\frac{\ln \tau(\lambda)}{L} \quad (5)$$

L is the thickness of the PET film used to obtain an intrinsic transmission coefficient $\tau(\lambda)$ and consequently an accurate $A(\lambda)$ dependence with wavelength.

The internal source S_p on the principal P control volume is (Eq.6):

$$S_p = - \int_{\Delta t V} \nabla \cdot \vec{\phi}(y) dv dt = - \int_{\Delta t S} q_r dS dt \quad (6)$$

S are the surfaces of the control volume for which normal are collinear to the assumed main incident flux direction, see Figure 11.

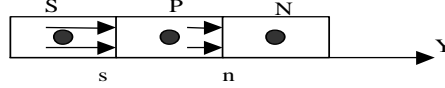


Fig.11- Radiative internal transfer

Finally the S_p formulation is expressed by (Eq.7):

$$S_p = \phi(x, y=0, z) \left[\tau_{\lambda}^{\frac{y_s}{L}} - \tau_{\lambda}^{\frac{y_n}{L}} \right] \quad (7)$$

In a next step, the integration of (Eq.1) over all the control-volumes leads to a linear equations system, which is solved iteratively using the line by line Gauss Seidel method in the y direction of range to obtain a three-dimensional system resolved by the TDMA algorithm.

4.3 Validation of the numerical model :

The numerical model is validated for the analytical case of a semi-infinite partially transparent solid [15], submitted to an uniform incident heat flux (q''_o). Its value is evaluated using (Eq.3), considering the entire spectrum and all the irradiated sheet surface (Eq.8).

$$q''_o = k_{rf} \frac{S_H}{S_R} F_{H-R} (\varepsilon_{moy} \sigma T_{fil}^4) \quad (8)$$

In these specific conditions, the temperature distribution across the thickness (y axis) versus time is computed using Laplace's transforms in order to solve the one-dimensional energy equation with the term source per unit volume, $q''_o''' (= q''_o'' A e^{-Ay})$ and considering adiabatic borders. A corresponds to an average absorption coefficient (Eq.9), evaluated from (Eq.5) with an average PET's transmittivity [16] :

$$\bar{\tau} = \frac{\Delta \lambda}{\int_{\Delta \lambda} M_{\lambda}^o(T_{fil}) d\lambda} \quad (9)$$

The solution is (Eq.10):

$$T(y,t) = T_{ini} - \frac{q''_o''}{kA} e^{-Ay} + q''_o'' \sqrt{\alpha t} \operatorname{erfc} \left(\frac{y}{2\sqrt{\alpha t}} \right) + \frac{q''_o''}{2kA} e^{A^2 \alpha t + Ay} \operatorname{erfc} \left(A\sqrt{\alpha t} + \frac{y}{2\sqrt{\alpha t}} \right) + \frac{q''_o''}{2kA} e^{A^2 \alpha t - Ay} \operatorname{erfc} \left(A\sqrt{\alpha t} - \frac{y}{2\sqrt{\alpha t}} \right) \quad (10)$$

where T_{ini} is the initial temperature.

Analytical and numerical solutions are compared for a 100x100 mm² sheet of 200 mm thickness. Its front surface is subjected to an incident radiation (9) considering a filament temperature about 1700K, corresponding to an average tungsten emissivity about 0.26 and an absorption coefficient of 2660 m⁻¹, for a wavelength delimited between 0.2 and 10 μm. The view factor in this case, between the strip heater and the sheet is evaluated to 0.53.

In Figure 13, comparisons for the temperature versus thickness are shown. The agreement is fair. The error is less than 2%.

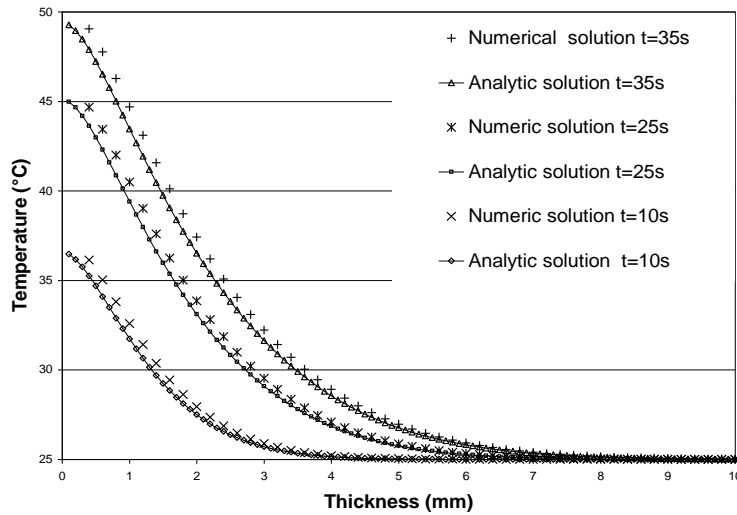


Fig. 13- Comparison between numerical and analytical temperatures versus thickness

4-4 PET Sheet's heating simulation

After the validation of the model, heating of thin sheets is now performed.

The predicted temperature using numerical simulations are compared to experimental temperature measurements in the case of a PET sheet of 1.5 mm thickness. The heating time is 35s, corresponding to typical heating times for industrial processes.

Boundary conditions are given below (Eq.14):

$$-k \left(\frac{\partial T}{\partial y} \right)_{y=0} = -k \left(\frac{\partial T}{\partial y} \right)_{y=e} = h(T_S - T_\infty) \quad \left(\frac{\partial T}{\partial x} \right)_{x=0,l} = \left(\frac{\partial T}{\partial z} \right)_{z=0,H} = 0 \quad (14)$$

An uniform convection coefficient is applied to the back and the front faces (estimated to $10 \text{ W m}^{-2} \text{ K}^{-1}$) [17].

The numerical modelisation leads to the following temperature distribution across the sheet thickness, in particular at the sheet centre (see Figure 14).

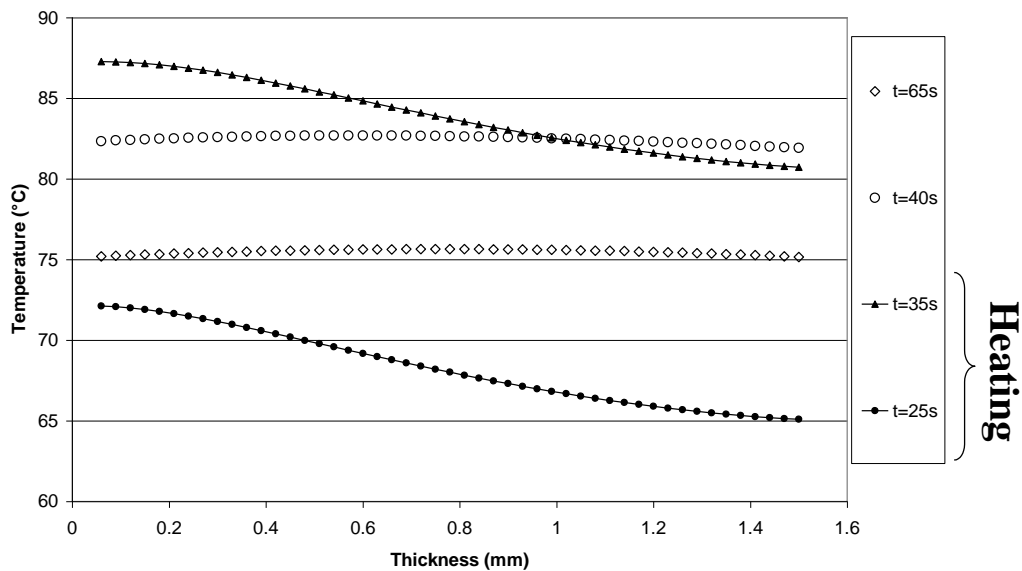


Fig. 14-Numerical Temperature distribution across the thickness

During the heating time, a constant temperature gradient across the thickness, equal to 7°C appears. Then, as soon as the heating is switch off, the temperature difference between the front and the back faces rapidly decreases. Five seconds are sufficient to observe the establishment of an equilibrium temperature level all across the thickness. It provides a confirmation of the temperature increase, recorded experimentally from the back face as the natural cooling starts.

The comparison between experimental and numerical results, for the temperature profile versus z axis is plotted in Figure 15.

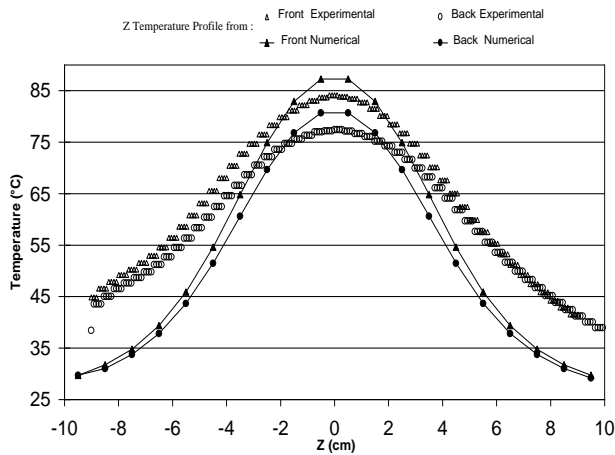


Fig.15- Gradient Temperature

Points localised near the sheet centre and in front of the heater (in a circle of 2cm diameter), the difference between the two temperature results is less than 2%. For the other part of the sheet, the discrepancy is more important. This observation is valid for both front and back faces of the sheet. This difference is firstly due, to the incident flux distribution on the irradiated face, more than the assumption, permitting the flux absorption only normally to the incident surface. Several reasons could explain this inaccurate incident front conditions. In particular the numerical geometry of the strip surface assumed to be equivalent to the radiative cylindrical heater surface. Previous workers [18], have shown a non-negligible quartz tube effect; denoting a refraction of the radiative beam from the tungsten filament centred in the quartz tube. This will lead an increase of the dispersion angle of the radiant heat flux.

In figure 16, the temperature profile versus time is plotted. The same remark is still available with the temperature localisation on the sheet. During the heating stage, numerical temperature evolutions are linear, which do not represent the experimental measurement. Comparisons during the cooling stage, exhibits a more important natural convection transfer for computed results.

CONCLUSION

Preliminary investigations of the infrared heaters properties (spatial and spectral) fitted with diffuse reflectors, allows to consider them as an isotropic radiative source. The interaction between these lamps and PET sheet has been observed, using an infrared camera. The temperature distribution from the back and the front face of the sheet has permit to estimate the gradient temperature at the heating switch off. Advantages of the infrared camera must be emphasise here, offering the capability to record spatial and transient surface temperature distribution, during heating and cooling stage. The heating stage of the PET sheet, submitted to

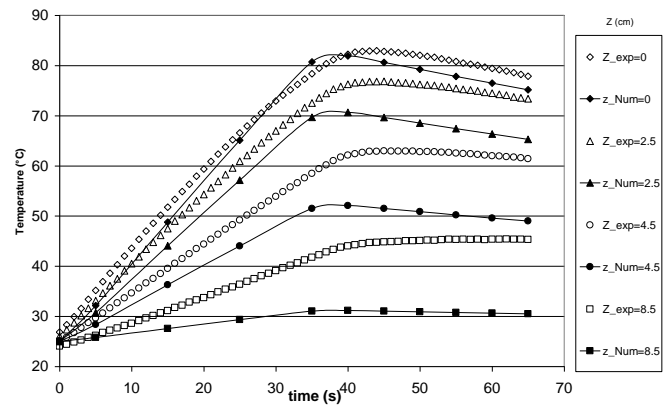


Fig.16- Transient Temperature from the back face.

an industrial infrared heater, is taking account with the one dimensional Beer-Lambert law, computed with a control volume model. Considering an efficiency reflector coefficient, the comparison between experimental and numerical results presents discrepancies. Further developments will permit, to take better into account the real interaction between PET preform and infrared heaters and the oven's environment :

- defining the reflector efficiency
- observing transfer convection
- modelling tubular PET preforms

Acknowledgements

This work is supported by PERRIER-VITTEL COMPANY. Special thanks go to G. Denis, A. Contal and J-P. Arcens.

References

- [1] C. Lindenlaub, Thermoformage , Techniques de l'Ingénieur, A3660. (1982)- in French
- [2] Y. Le Maout, F. Schmidt, M. El Hafi, Measurement and Calculation of Preform Infrared Heating , 4th Int. Workshop on Adv. Infrared Tech. and App.-Firenze, Sept, (1997)
- [3] S. Monteix, R. Diraddo, F. Schmidt, Profiles Infrared Radiative Heating in blow molding and Thermoforming , PPS'98- Noth American Meeting Toronto, Aug 17-19. (1998)
- [4] K. Hartwig, Simulation of the Stretch-Blow Molding Process and Characterization of the Relevant Material Behavior, Dissertation, RWTH, Aachen. (1996)
- [5] M. Lallemand, A. Souffiani, Mesure de Température dans les milieux semi-transparents Rev. Gen. Therm. (HS95), Vol 34, p. 69-85.-in French
- [6] N. Haji, J. E. Spruiell, Radiation Pyrometry on Semitransparent Sheets. I: Gray Media, Polym. Eng. Science, Vol.34, No.2, (1994), 116 – 121.
- [7] M. D. Shelby, Effects of Infrared Lamp Temperature and Other Variables on the Reheat Rate of PET, Antec'91, (1991), p.1420 – 1424.
- [8] J.F Agassant, P. Avenas, J. Ph Sergent, La mise en forme des matières plastiques, Ed. Technique et Documentation- Lavoisier. (1986). -in French
- [9] S. V. Patankar, Numerical Heat Transfer and Fluid Flow, Ed. Mc Graw Hill New-york. (1980)
- [10] K. Esser, Infrared Radiation in the Processing of Plastics: Precise Adjustment- the key to Productivity, Advances in Polymer Technology, Vol.7, No.2, (1987), p.89 – 128.
- [11] P. Lebaudy, Etude et Simulation de la répartition des températures dans un cylindre creux de PET soumis a un rayonnement infra-rouge, Université de Rouen. (1989) -in French
- [12] A. Denis, Etude expérimentale et modélisation du chauffage par rayonnement infrarouge de polymères semi-cristallins: influences des centres diffusants, Université de Rouen. (1995) – in French
- [13] R. Rammohan, Efficient Evaluation of Diffuse View Factors for Radiation, Int. J. Heat Mass Transfer, Vol.39, No.6, (1996), p.1281 – 1286.
- [14] S. Harmand, Contribution a la modélisation des échanges radiatifs entre un champ d'émetteurs infrarouges et un corps en déplacement, Université de Valenciennes et du Hainaut Cambresis, (1990) -in French
- [15] A. De Wriendt, La transmission de la Chaleur Voll, tome 1, Ed.2, G. Morin. -in French
- [16] R. Siegel, J.R. Howel, Thermal Radiation Heat Transfer, 3rd Ed Hemisphere/ Taylors and Francis, Washington. (1992)
- [17] J.F. Sacadura, Initiation aux Transferts Thermiques, Ed Lavoisier. (1973) -in French

- [18] T.L. Turner, Numerical and experimental Analyses of the Radiant Heat Flux Produced By Quartz Heating Systems, NASA Technical Paper 3387, Langley Research Center, Virginia, March 1994